

Citation for the published version:

Zhu, H., Yang, Y., Zhu, X., Sun, Y., & Wong, S. W. (2018). Miniaturized Resonator and Bandpass Filter for Silicon-Based Monolithic Microwave and Millimeter-Wave Integrated Circuits. *IEEE Transactions on Circuits and Systems I: Regular Papers*, 65 (12), 4062-4071. DOI: 10.1109/TCSI.2018.2839701

Document Version: Accepted Version

Link to the final published version available at the publisher:

<https://doi.org/10.1109/TCSI.2018.2839701>

© 2018 IEEE. Personal use of this material is permitted. Permission from IEEE must be obtained for all other uses, in any current or future media, including reprinting/republishing this material for advertising or promotional purposes, creating new collective works, for resale or redistribution to servers or lists, or reuse of any copyrighted component of this work in other works.

General rights

Copyright© and Moral Rights for the publications made accessible on this site are retained by the individual authors and/or other copyright owners.

Please check the manuscript for details of any other licences that may have been applied and it is a condition of accessing publications that users recognise and abide by the legal requirements associated with these rights. You may not engage in further distribution of the material for any profitmaking activities or any commercial gain. You may freely distribute both the url (<http://uhra.herts.ac.uk/>) and the content of this paper for research or private study, educational, or not-for-profit purposes without prior permission or charge.

Take down policy

If you believe that this document breaches copyright please contact us providing details, any such items will be temporarily removed from the repository pending investigation.

Enquiries

Please contact University of Hertfordshire Research & Scholarly Communications for any enquiries at rsc@herts.ac.uk

Miniaturized Resonator and Bandpass Filter for Silicon-Based Monolithic Microwave and Millimeter-Wave Integrated Circuits

He Zhu, Yang Yang, *Senior Member, IEEE*, Xi Zhu, *Member, IEEE*, Yichuang Sun, *Senior Member, IEEE*, and Sai-Wai Wong, *Senior Member, IEEE*

Abstract—This paper introduces a unique approach for the implementation of a miniaturized on-chip resonator and its application for 1st-order bandpass filter (BPF) design. This approach utilizes a combination of a broadside-coupling technique and a split-ring structure. To fully understand the principle behind it, simplified *LC* equivalent-circuit models are provided. By analyzing these models, guidelines for implementation of an ultra-compact resonator and a BPF are given. To further demonstrate the feasibility of using this approach in practice, both the implemented resonator and the filter are fabricated in a standard 0.13- μm (Bi)-CMOS technology. The measured results show that the resonator can generate a resonance at 66.75 GHz, while the BPF has a center frequency at 40 GHz and an insertion loss of 1.7 dB. The chip size of both the resonator and the BPF, excluding the pads, is only 0.012 mm² (0.08 \times 0.144 mm²).

Index Terms—bandpass filter (BPF), Bi-CMOS, miniaturization, on-chip resonator, RFIC, microwave, millimeter-wave, Silicon-Germanium (SiGe).

I. INTRODUCTION

SILICON Silicon-based monolithic microwave integrated-circuit (MMICs) design has advanced by leaps and bounds over the last half-century. Currently, wireless systems are approaching a performance level that will enable an exciting new range of applications, such as full -duplex radios [1], phased arrays [2] and passive imaging [3]. The performance of MMICs is normally evaluated regarding a key criterion, which is the fabrication cost. Although enormous amount of effort has been made to improve the overall performance of active devices, namely transistors, by scaling,

and to implement low-loss transmission lines, high-*Q* inductors and transformers [4]-[6], there are still spaces for innovation in terms of cost reduction. As the die size of an MMIC is often primarily constrained by the physical dimensions of passive devices, miniaturization of passive devices becomes one of the most critical issues for low-cost MMIC design. For low-frequency designs, although both active inductor and lumped element approaches have been well explored for ultra-compact MMIC designs [7]-[8], none of these approaches seems to effectively work as the operation frequency is pushed into the millimeter-wave region. On the other hand, the conventional way to implement on-chip passive devices is to simply transfer the classical microwave planar structures that have been used for years into MMIC designs. Unfortunately, this approach usually results in a relatively large die footprint, which is not ideal for a cost-constrained application [9], [10]. Therefore, design of low-cost and high-performance MMICs are urgently looking for solutions that can be used to implement miniaturized passive devices.

Different design techniques for passive-device miniaturization can be grouped into two general categories, lumped- and distributed-element designs, which is to name the two. It is noteworthy that both designs are proposed to satisfy different design specifications. It is not a matter of the one eliminating the other, but either being complementary or serving different situations. Perhaps, lumped-element-based approach is more popular for on-chip passive design at microwave frequency, which has been well documented in [11]. A variation of this approach is the so-called capacitive loading technique, which uses grounded capacitors to reduce the required overall electrical length. Consequently, the die size can be dramatically reduced [12]-[13]. In addition, an MIM capacitor is not only provided in almost every RF Si-based technology but is also inherently much more compact than its interdigital-based counterparts, thus this approach has become a natural choice for device miniaturization. Another variation is to fully utilize the 3-D metal stack-up provided in any standard silicon-based technologies [14]-[18]. In deep-submicron technology, at least 7 metal layers are offered with thick aluminum layers that are particularly suitable for implementation of passive devices. One of the most successful design examples to be found in the literature is to use this approach to implement 3-D inductors, which has been proved

Manuscript received XXX; revised XXXX; accepted XXXX. This research is supported by the Australian Research Council DE160101032.

H. Zhu, Y. Yang, and X. Zhu are with the School of Electrical and Data Engineering, Global Big Data Technology Center (GBDTC), University of Technology Sydney, Ultimo, NSW 2007, Australia. (E-mail: xi.zhu@uts.edu.au)

Y. Sun is with the School of Engineering and Technology, University of Hertfordshire, Hatfield, Hertfordshire, AL10 9AB, UK. (E-mail: y.sun@herts.ac.uk)

S.-W. Wong is with College of Information Engineering, Shenzhen University, Shenzhen 518060, China.

Color versions of one or more of the figures in this paper are available online at <http://ieeexplore.ieee.org>.

Digital Object Identifier 0000

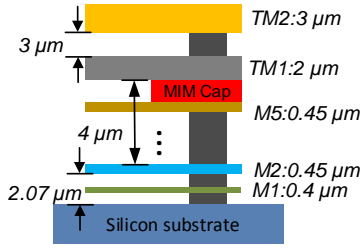


Fig. 1 Metal stack-up of the selected 0.13- μm (Bi)-CMOS technology.

to be very useful for ultra-compact low-noise amplifier (LNA) and voltage-controlled oscillator (VCO) designs [14], [16]. The second category is the distributed-element-based approach. Among different design approaches under this category, there is an emerging one, namely slow-wave coplanar waveguide (S-CPW), which takes advantages of using both 3-D and slow-wave structures [19]-[25]. Although this one is still in an infant stage, several interesting designs using this approach have already been presented in the literature, including not only resonators [19], transmission lines [20]-[22], and power dividers [22]-[23], but also accurate devices modelling for S-CPW implementation in the standard Si-based technologies [24]-[25].

In this work, design of a broadside-coupled split-ring resonator (BCSRR) is presented, followed by the integration with metal-insulator-metal (MIM) capacitors for a bandpass filter (BPF) implementation, as a design example of a miniaturized passive device. In addition, simplified LC equivalent-circuit models for both the BCSRR and BPF are developed that are used for fundamental analysis, so that the principle behind the presented approach can be fully explored. To prove that the presented concept is functional in practice, both designs are implemented and fabricated in a standard (Bi)-CMOS 0.13- μm technology. A good agreement between the simulation and measurements has been achieved. The rest of this paper is organized in the following way. In Section II, the proposed BCSSR and its application for a BPF design is presented. In Section III, the measured results are presented. Finally, a conclusion is drawn in Section IV.

II. DESIGN OF BROADSIDE-COUPLED SPLIT-RING RESONATOR

A. The presented electromagnetic structure

A standard 0.13- μm (Bi)-CMOS SiGe technology is used in the design, which provides not only high-performance transistors (with f_t of 200 GHz), but also 7 metal layers with aluminum as the thick top two metal layers. The additional MIM layer is placed between TM1 and M5. A cross-section view of the metal stack-up is given in Fig. 1. In addition, the height of the silicon substrate is 200 μm [12], [26], [27]. The dielectric constant of SiO_2 is 4.1 and the loss tangent is 0.01.

B. Analysis and design of the presented resonator

In order to further leverage the benefits of using a slow-wave-based approach for miniaturized passive-device design, a unique electromagnetic (EM) structure, namely a BCSSR, is

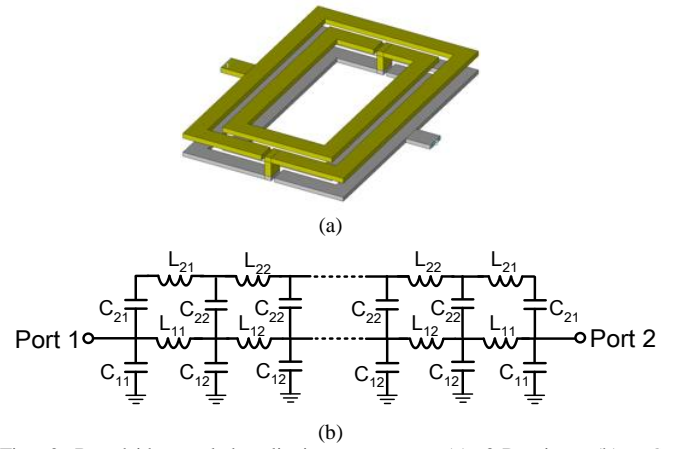


Fig. 2 Broadside-coupled split-ring resonator: (a) 3-D view, (b) LC equivalent-circuit of the resonator.

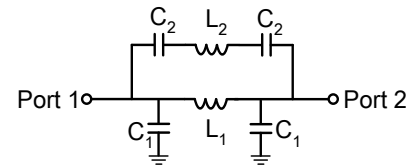


Fig. 3 Simplified LC -equivalent circuit presented in Fig. 2(b).

proposed in this work. The 3-D view of this structure is shown in Fig. 2(a). As illustrated, the presented structure consists of two split rings, which are both vertically folded using the top two metal layers, but with opposite orientations. To understand the fundamental principle of this structure, the LC equivalent-circuit model is given in Fig. 2(b). Since the metallic line behaves as an inductive conductor and capacitive couplings exist between the two split rings, the structure can be modeled by an equivalent LC -circuit as shown in Fig. 2(b). The split-ring resonator can be divided into n sections and modeled by n -stage inductances L_{11} , L_{12} , L_{21} , and L_{22} , where the first and n th stage of inductance equals to L_{11} and L_{21} while the other $n-2$ stages are L_{12} and L_{22} . For the coupling characteristics, the capacitances C_{11} and C_{12} account for the electrical coupling between the metallic line and the ground, and C_{21} and C_{22} stand for the mutual electrical coupling between the two split rings. In order to effectively demonstrate the insight of the presented structure, the complex lumped-element circuit can be simplified by merging several elements with similar functions into one component. For example, all n stages of grounded capacitances are small and equal to each other except for the first and n th stages with very small differences in value that can be neglected. Therefore, it is possible and practical to represent all the ground capacitances using one capacitor with a value of $n \cdot C_{21}$. In this case, the n -stage LC -model can be simplified to a 2-stage structure, which is shown in Fig. 3. As can be observed, the n -stage of inductances of the split-ring resonators can be expressed by two inductances L_1 and L_2 , and the mutual coupling between the metallic lines and ground and the mutual coupling between the two resonators are expressed by C_1 and C_2 , respectively.

Since the circuit is fully symmetrical, it is possible to describe its transmission characteristics by adopting the even- and odd-mode analysis method. The even-mode and odd-mode lumped-element equivalent circuits are presented in

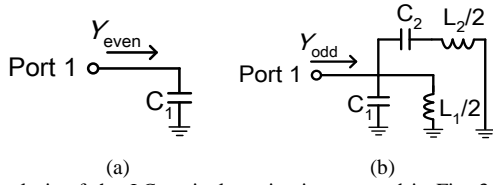


Fig. 4. Analysis of the LC-equivalent circuit presented in Fig. 3: (a) even-mode, (b) odd-mode.

Figs. 4(a) and 4(b), respectively. For the even mode, the symmetric plane in the middle is considered as a perfect magnetic wall, while for the odd mode, the middle plane is treated as a perfect electrical wall (virtual ground).

The resonator can be modeled as a reciprocal two-port network by its admittance matrix $[Y]$

$$[Y] = \begin{pmatrix} \frac{Y_{even} + Y_{odd}}{2} & \frac{Y_{even} - Y_{odd}}{2} \\ \frac{Y_{even} - Y_{odd}}{2} & \frac{Y_{even} + Y_{odd}}{2} \end{pmatrix} \quad (1)$$

where Y_{even} and Y_{odd} represent the even- and odd-mode input admittances

$$Y_{even} = j\omega C_1 \quad (2)$$

$$Y_{odd} = j\omega C_1 - j \frac{1}{\omega L_1/2} + j \frac{\omega C_2}{1 - \omega^2 L_2 C_2/2} \quad (3)$$

Then the scattering parameters of the two-port network can be expressed as [10]

$$S_{21} = \frac{Y_o(Y_{even} - Y_{odd})}{(Y_o + Y_{odd})(Y_o + Y_{even})} \quad (4)$$

$$S_{11} = \frac{Y_o^2 - Y_{even}Y_{odd}}{(Y_o + Y_{odd})(Y_o + Y_{even})}$$

where Y_o is the load admittance. For the proposed resonator with two tapped ports, it is possible to find the transmission zero by solving $S_{21} = 0$. In this design, the reflection pole within the stopband can be found from

$$Y_{even} - Y_{odd} = 0 \quad (5)$$

Replacing Y_{even} and Y_{odd} in (5) using (2) and (3), one can easily find the position of the transmission zero located at

$$\omega_o = \sqrt{\frac{2}{C_2(L_1 + L_2)}} \quad (6)$$

It is clearly seen from (6) that the position of the reflection pole ω_o is determined by the mutual coupling C_2 and the overall inductance of the metal strip $L (= L_1 + L_2)$. Since C_2 represents the mutual coupling between the top and bottom split rings, its value is limited to a small range due to practical implementation issues, where the resonant frequency is mainly determined by L . Therefore, it is possible to select an appropriate value of C_2 first and then find L using (6).

Meanwhile, it is also important to investigate the quality factor (Q -factor) of the resonator, since it is closely related to the bandwidth and loss of the resonator. The Q -factor can be expressed as:

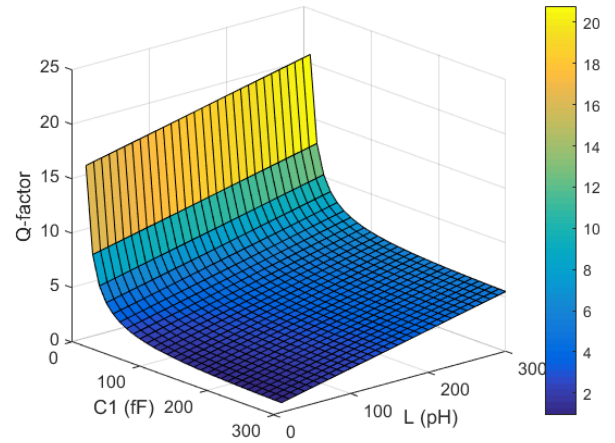


Fig. 5. 3-D mapping of the Q -factor of the proposed BSCCR against C_1 and L .

$$Q = \frac{2b}{Y_o} \quad (7)$$

while b is estimated as:

$$b = \frac{\omega_o}{2} \cdot \frac{\partial \text{Im}[Y_{11}(\omega_o)]}{\partial \omega} \quad (8)$$

Here, b is the susceptance slope parameter of the resonator, and $Y_{11}(\omega_o)$ is the value of Y_{11} at the resonant frequency ω_o in equation (1). Considering (1)-(3) and (6)-(8), the Q -factor of the resonator can be expressed as

$$Q = \frac{\omega_o}{Y_o} \cdot \left(C_1 + \frac{1}{\omega_o^2 L_1} + \frac{C_2 + \omega_o^2 L_2 C_2^2/2}{(1 - \omega_o^2 L_2 C_2/2)^2} \right) \quad (9)$$

It is observed from (9) that the Q -factor is related to C_1 , C_2 and L , as well as the resonance ω_o . Since the Q -factor is varied against ω_o in a very complex way, it is difficult to see its insight; however, the relation between the Q -factor and other related parameters can be found in a straightforward way, if the frequency is fixed. As an example, a 3-D mapping of the Q -factor against the capacitance C_1 and the inductance L at 50 GHz is given in Fig. 5. As illustrated, the Q -factor can be improved, if a smaller capacitance is selected.

C. Analysis and design of a BPF using BCSRR

Using the previously analyzed EM structure along with two metal-insulator-metal (MIM) capacitors, the design of a BPF is presented in this section. The simplified LC-equivalent circuit model of the filter is given in Fig. 6. The structure can be regarded as a 1st-order BPF, which has two cascaded capacitors and a BCSRR. Similar to the BCSRR, the BPF can also be analyzed using even- and odd-mode analysis method duo to its symmetry. The equivalent circuits are shown in Fig. 7(a) and (b). The even- and odd-mode input admittances Y'_{even} and Y'_{odd} can be expressed as

$$Y'_{even} = \frac{j\omega C_p \cdot Y_{even}}{j\omega C_p + Y_{even}} \quad (10)$$

$$Y'_{odd} = \frac{j\omega C_p \cdot Y_{odd}}{j\omega C_p + Y_{odd}} \quad (11)$$

Similar to (5), the transmission zeros of the filter can be found by solving

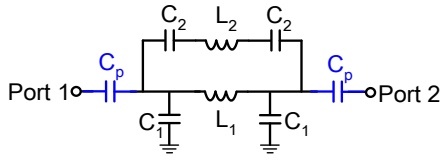


Fig. 6. Simplified LC-equivalent circuit model of the proposed BPF using the proposed BCSRR.

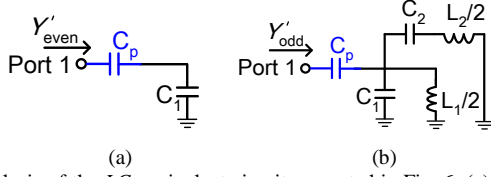


Fig. 7. Analysis of the LC-equivalent circuit presented in Fig. 6: (a) even mode, (b) odd mode.

$$Y'_{even} - Y'_{odd} = 0 \quad (12)$$

It is obvious that $\omega = 0$ is a root of equation (12), indicating that a transmission zero is located at DC. Compared with Fig. 3, two additional capacitors, namely C_p , are cascaded with the resonator in the design. These capacitors are not only used for DC blocking, but also able to generate an additional resonance of $\bar{\omega}_o$, which is different from the pole of the resonator, ω_o .

To investigate the coupling coefficient and the resonance of the BPF, a modified LC-equivalent circuit model for the BPF is presented in Fig. 8. As shown, a shunted negative capacitance $-C_{pa}$ is added to be a part of an L-shape network, so that sufficient coupling can be provided to the filter [28]. However, this capacitor will affect the resonance of the filter. Therefore, another shunted capacitor C_{pa} is required to be included in the modified model, which is also shown in Fig. 8. In this case, the effect of the series capacitor C_p on the resonance can be equivalently measured by the shunt capacitor C_{pa} .

To precisely analyze the effect of the cascaded capacitors C_p on the resonance of the BPF, the even- and odd-mode analysis method is applied, as given in Fig. 9(a) and (b). In this case, the resonance of the BPF can be found out by calculating the resonance of the modified circuit model. The value of C_{pa} is related to C_p , which is parameterized as [28]:

$$C_{pa} = \frac{C_p}{1 + (\omega C_p / Y_o)^2} \quad (13)$$

The relation between the original capacitance C_p and its equivalent capacitance C_{pa} is illustrated in Fig. 10 under different resonance frequencies. In this case, the corrected even- and odd-mode input admittances of the BPF, namely \bar{Y}_{even} and \bar{Y}_{odd} , can be expressed as

$$\bar{Y}_{even} = Y_{even} + jB_{pa} \quad (14)$$

$$\bar{Y}_{odd} = Y_{odd} + jB_{pa} \quad (15)$$

The transmission zeros of the filter can be found by solving

$$\bar{Y}_{even} - \bar{Y}_{odd} = 0 \quad (16)$$

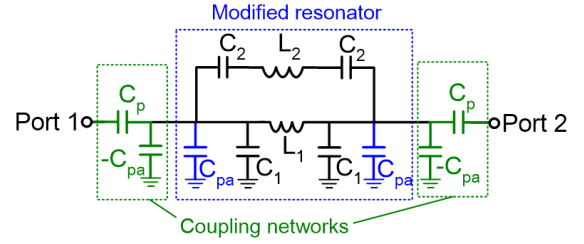


Fig. 8. Modified LC-equivalent circuit model for the BPF presented in Fig. 6.

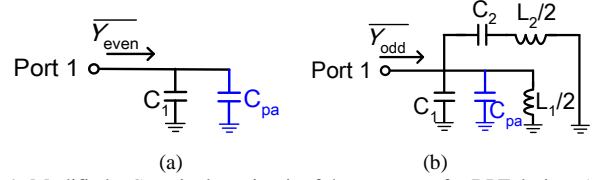


Fig. 9. Modified LC-equivalent circuit of the resonator for BPF design: (a) even-mode, (b) odd-mode.

Substituting (14) and (15) into (16), one can get:

$$\bar{Y}_{even} - \bar{Y}_{odd} = Y_{even} - Y_{odd} \quad (17)$$

It can be found from (17) that the criteria for solving the transmission zero of the BPF is exactly the same as for the resonator, which is given in (6). Thus, the transmission zero of the BPF is placed at exactly the same position as the reflection pole of the resonator, that is

$$\omega_{tz} = \omega_o \quad (18)$$

On the other hand, since the resonant frequency within the passband is produced by the odd-mode excitation, it is possible to find the position of $\bar{\omega}_o$ by solving $\bar{Y}_{odd} = 0$. Considering equation (15), the following formula can be found:

$$j\omega C_{pa} + j\omega C_1 - j\frac{1}{\omega L_1/2} + j\omega\frac{C_2}{1 - \omega^2 L_2 C_2/2} = 0 \quad (19)$$

After solving (19), the angular frequency of the resonance of the BPF is found to be located at

$$\bar{\omega}_o = \sqrt{\frac{2(-s + \sqrt{s^2 + t})}{t}} \quad (20)$$

where

$$s = \frac{(C_1 + C_{pa})L_1 + (L_1 + L_2)C_2}{2} \quad (21)$$

$$t = L_1 L_2 C_2 (C_1 + C_{pa}) \quad (22)$$

As observed from (20)-(22), the resonance frequency of the BPF $\bar{\omega}_o$ is related to all parameters of C_1 , C_2 , C_{pa} , L_1 and L_2 . Although it seems to be complicated that there are five variables in (20)-(22), some of them can be determined first by fixing the position of the transmission zero ω_{tz} . Once the ω_{tz} is fixed, the values of C_2 and $L_1 + L_2$ are also determined. The selection process of C_2 , L_1 and L_2 is similar to the one previously discussed for the resonator design, which is not repeated here. In addition, the Q -factor and the fractional bandwidth (FBW) of the BPF can also be controlled by the L-shape coupling networks. To that end, two conditions need to

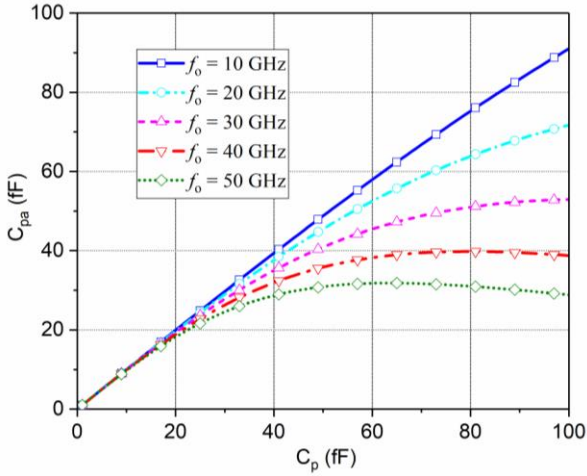


Fig. 10. Relation between the original capacitance C_p and the effective capacitance C_{pa} .

be satisfied at the same time: the resonant condition, which is given in (20), and the coupling condition. For the coupling condition, the Q -factor of the filter \bar{Q} is determined by the susceptance slope parameter of the BPF, which is calculated by

$$\bar{Q} = \frac{2\bar{b}}{Y_o} \quad (23)$$

where

$$\bar{b} = \frac{\bar{\omega}_o}{2} \cdot \frac{\partial \text{Im}[Y_{11}(\bar{\omega}_o)]}{\partial \omega} \quad (24)$$

Here, \bar{b} is the susceptance slope parameter of the resonator considering the effect of cascaded C_p and BCSSR. It is clearly seen from (23) and (24) that the intrinsic Q -factor of the resonator in the BPF can be easily tuned by controlling \bar{b} . Moreover, as previously mentioned, the values of capacitance C_2 and inductance L are determined as ω_{tz} are fixed. Therefore, it is possible to select the appropriate values for C_{pa} and L to find the desired resonance $\bar{\omega}_o$ and the Q -factor.

It is noted that the cascaded capacitance C_p does not change the unloaded Q -factor of the BCSSR at all, but it will affect the external Q -factor of the filter Q_{ex} (also known as loaded Q -factor). The external Q -factor of the filter Q_{ex} is related to the bandwidth of the filter. As illustrated in Fig. 11, the simulated frequency responses of the BPF with different external Q -factors are presented. The bandwidth of the designed BPF can be greatly varied without changing the center frequency and the position of transmission zero, which makes the presented approach very flexible for circuit designs.

The scattering parameters of both the BPF and the resonator can be plotted using modified equation (4) by replacing Y_{even} with \bar{Y}_{even} and Y_{odd} with \bar{Y}_{odd} . It is straightforward to verify that the position of resonance frequency $\bar{\omega}_o$ is inherently located at lower frequencies than the transmission zero ω_{tz} by comparing (20) with (6), which indicates that the transmission zero will locate at the upper-stopband of the BPF for harmonic suppression. Fig. 12 shows the simulated S-parameters of the presented resonator and BPF using the same lumped elements except for the inclusion

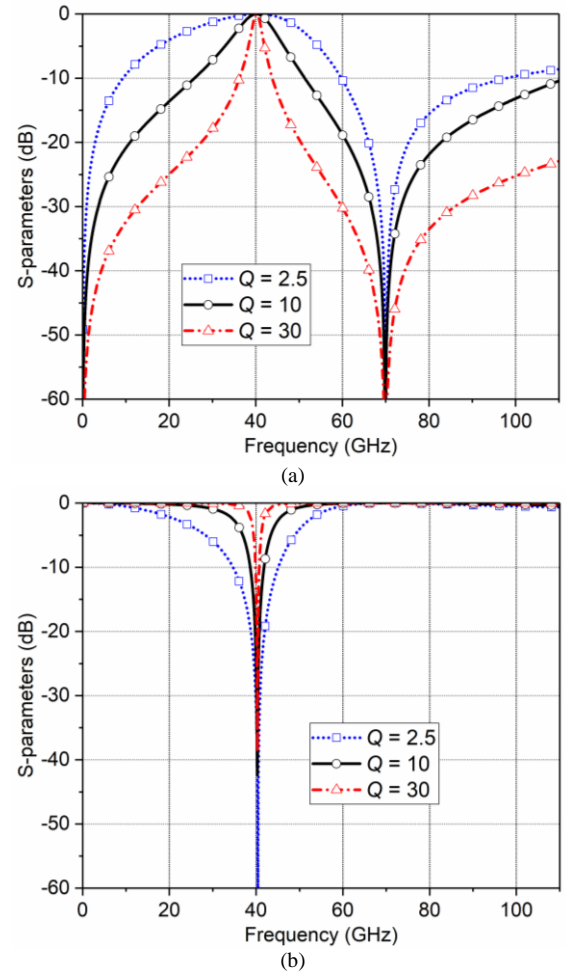


Fig. 11. Calculated results of the proposed BPF with different Q -factors: (a) $|S_{21}|$; (b) $|S_{11}|$.

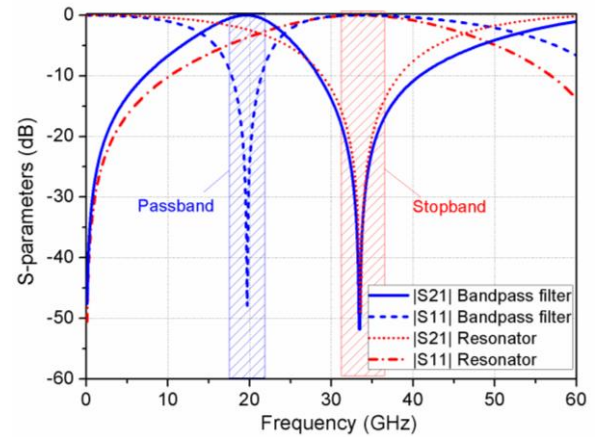


Fig. 12. Calculated S-parameters of the designed resonator and BPF using LC-equivalent circuit.

of C_p in the BPF. It is clearly seen that the transmission zeros created by the resonator and BPF are located at exactly the same position, which is at higher frequencies than the passband and thus forms the stopband of the BPF. Meanwhile, the positions of the transmission zero, resonance, external Q -factor and the bandwidth of the BPF can be easily controlled as discussed above. It is also noted that the resonance of the BPF is used to construct the passband, while the resonance of

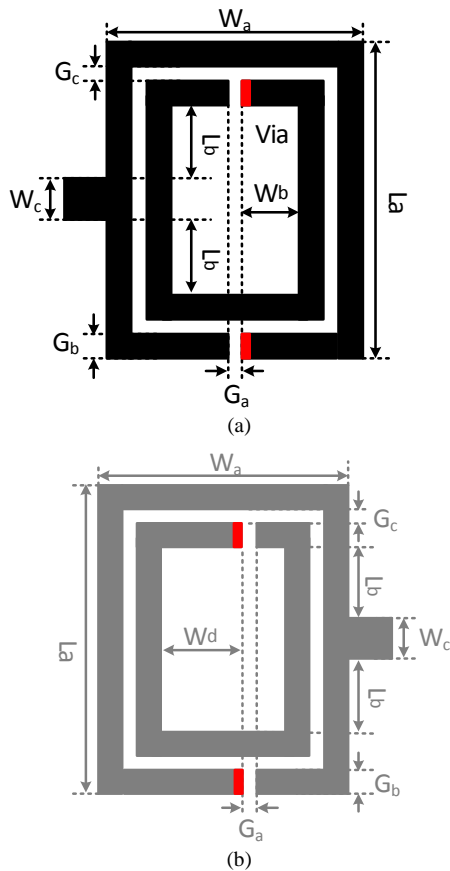


Fig. 13. 2-D view of the designed resonator: (a) TM2 layer, (b) TM1 layer.

the BCSSR is used for generating a notch, which are quite different.

D. Implementation of the presented resonator and BPF

To be able to verify the derived equations, both the resonator and the BPF are implemented in this section. The 2D-view of the presented resonator is shown in Fig. 13, of which the physical dimensions are given in Table I. As previously discussed, by varying the overall inductance of the metal strip, the resonance can be effectively controlled. As illustrated in Fig. 14(a), the resonance is shifted from 50 to 68 GHz as the variable L_a is varied from 140 to 180 μm . In addition, in Fig. 14(b), the tuning of resonance by means of variation of W_l is demonstrated.

On the other hand, the 3D-view of the implemented BPF is shown in Fig. 15. As previously analyzed, the cascaded capacitors, C_p could have an impact on the center frequency of the BPF. Thus, the simulated frequency responses of the filter in terms of $|S_{21}|$ and $|S_{11}|$ are given in Fig. 16. As illustrated, the center frequency of the filter can be tuned by changing the capacitance values. More importantly, as predicted in the previous section, the variation of capacitance has a marginal impact on the transmission zero, which enables an independent pole-zero adjustment.

To further demonstrate the design flexibility of using the presented approach, the 5-step design flow used in this work is summarized in Fig. 17. In Step 1, the variable G_2 , which is the width of the metal strips and the stacked metal layers, needs to be selected. In this work, only the top two metal layers are

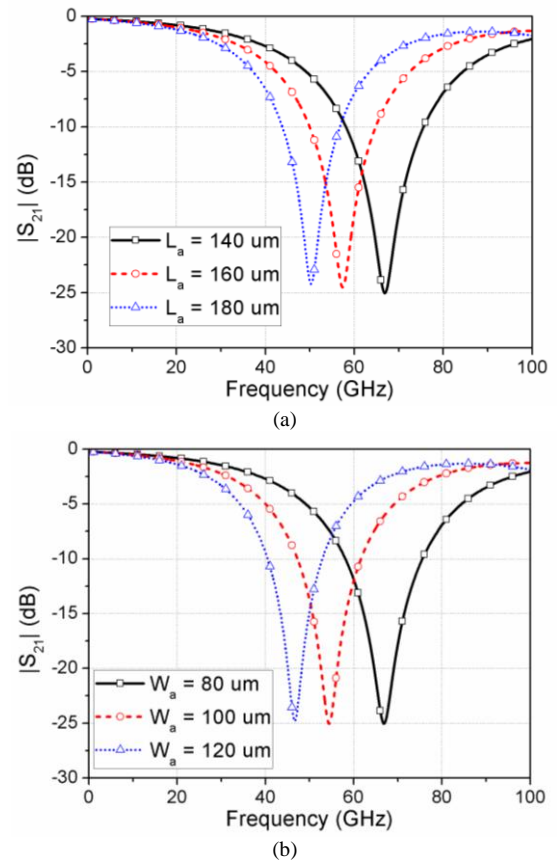


Fig. 14. Simulated S-parameters of the resonator: (a) the overall length L_a is swept; (b) the overall width W_l is swept.

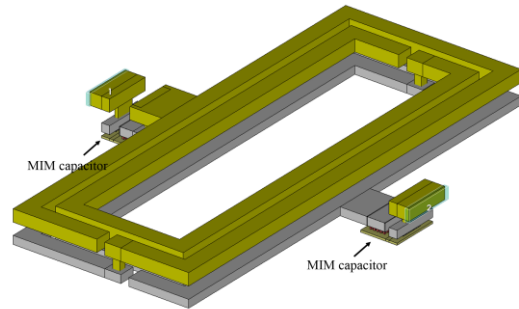


Fig. 15. 3-D view of the designed BPF using the resonator shown in Fig. 2.

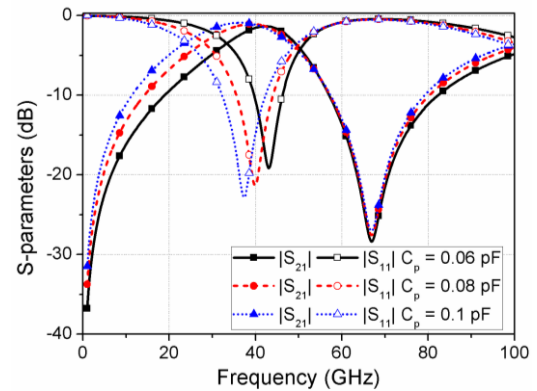


Fig. 16. Simulated S-parameters of the BPF with different cascaded capacitance values.

selected, although all the metal layers could be used to satisfy

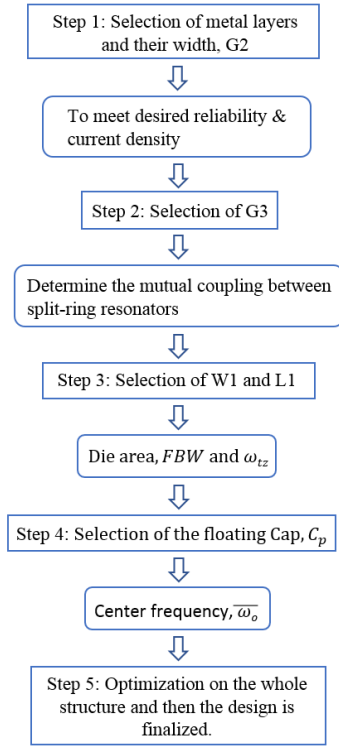


Fig. 17. Design flow used in this work.

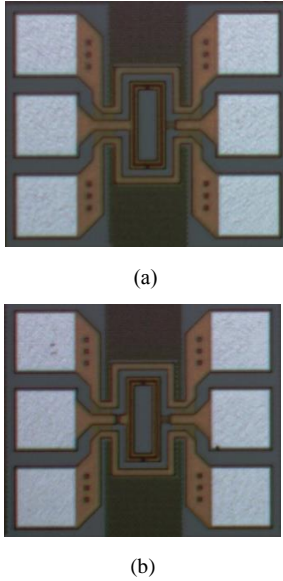
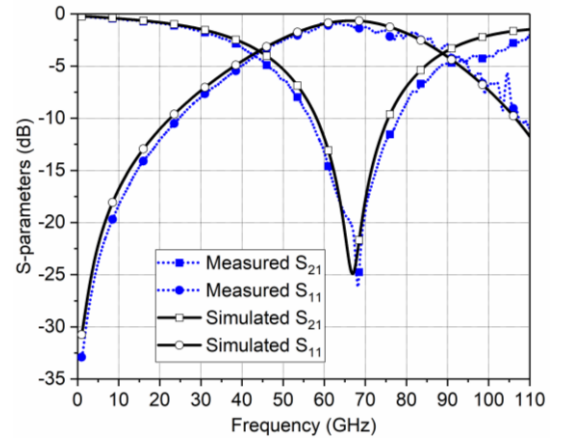
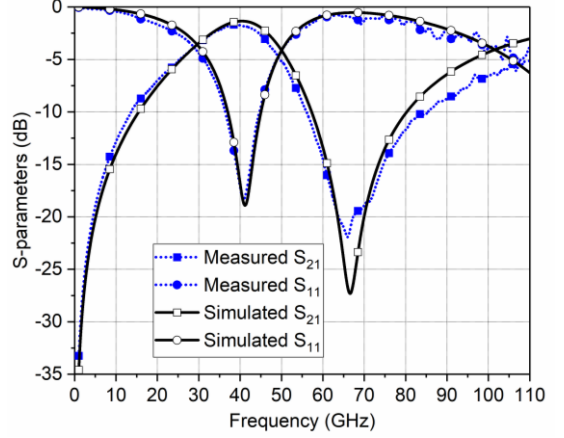


Fig. 18. Die photos of the design structures: (a) the resonator, (b) BPF.

different design specifications. The selected value for G_2 is $4 \mu\text{m}$ to ensure a good reliability and reasonable capability for current handling. Then, in Step 2, the mutual coupling between the two resonators needs to be determined by selecting a value for variable G_3 . Since the main motivation of this work is to design miniaturized passive devices, the minimum allowed gap between the metal strips is selected. In Step 3, for a constraint area, the width W_1 and the length L_a of the EM structure can be carefully optimized according to the results shown in Fig. 14. As illustrated in Figs. 12 and 16, the transmission zero of the BPF is independent of the value of C_p . Thus, in Step 4, the value of C_p can be determined based



(a)



(b)

Fig. 19. Measured S-parameters: (a) the resonator, (b) the BPF.

TABLE I PHYSICAL DIMENSIONS OF THE IMPLEMENTED RESONATOR.

W_a	W_b	W_c	W_d	L_a
$44 \mu\text{m}$	$11 \mu\text{m}$	$11.6 \mu\text{m}$	$17 \mu\text{m}$	$108 \mu\text{m}$
G_a	G_b	G_c	L_b	
$2 \mu\text{m}$	$4 \mu\text{m}$	$2 \mu\text{m}$	$38.2 \mu\text{m}$	

on the requirements of $\bar{\omega}_o$ and FBW of the BPF. Finally, the overall performance of the designed BPF can be re-optimized to fully satisfy all design specifications.

III. MEASUREMENT RESULTS

To evaluate the performance of the proposed resonator and BPF, both circuits are fabricated in a standard $0.13\text{-}\mu\text{m}$ SiGe technology. The chip photos are shown in Fig. 18. Excluding the pads, the chip size of both circuits is identical and is only $0.08 \times 0.144 \text{ mm}^2$. Using a vector network analyzer (VNA), ME7838A, from Anritsu, both circuits are measured via on-wafer G-S-G probing, from 1 GHz up to 110 GHz. Measurements were made by using conventional open-short-load-thru (OSLT) on-wafer calibration to move the reference planes from the connectors of the equipment to the tips of the RF probes.

For comparison, both the simulated and measured $|S_{21}|$ and $|S_{11}|$ (also known as return loss) of the resonator are plotted in Fig. 19(a). As illustrated, the simulated resonance appears at

TABLE II PERFORMANCE SUMMARY AND COMPARISONS WITH THE OTHER STATE-OF-THE-ART DESIGNS.

Ref.	Center frequency (GHz)	FBW (%)*	Insertion loss (dB)	Return loss (dB)	Die size (mm ²)	Q_u	Technology
[5]	60	17	4.1	15	0.29	23.7	0.13- μ m CMOS
[12]	60	27	4	22	0.16	15.3	0.18- μ m SiGe
[13]	31	23	2.4	13	0.024	15.5	0.13- μ m SiGe
[17]	65	18	3.1	16	0.074	18.3	0.18- μ m CMOS
[26]	33	18	2.6	15	0.038	17.3	0.13- μ m SiGe
[27]	33	42	2.6	20	0.031	15.1	0.13- μ m SiGe
This work	40	20	1.7	19	0.012	18.2	0.13-μm SiGe

Note: All FBW presented in this table is referred to return loss of better than 10 dB.

66.75 GHz with 25 dB attenuation, while the measured one has a resonance at 68.25 GHz with 27 dB attenuation. Thus, a fairly reasonable agreement between the EM simulation and measurements on the resonator is obtained. Moreover, both the simulated and measured S_{21} and S_{11} of the BPF are shown in Fig. 19(b). As illustrated, the BPF has a measured center frequency at 40.75 GHz with an insertion loss of 1.7 dB, while the simulated center frequency is located at 41.25 GHz with an insertion loss of 1.4 dB. In addition, the measured S_{11} is better than -10 dB from 36.5 GHz to 44.6 GHz. The discrepancy between the simulated and measured results and some ripples appeared in the tested results above 80 GHz are caused by the G-S-G pads and testing environment, which are not included in the EM simulation. In addition, up to 10 dBm input power is used to verify the linearity of the designed filter, and there is no compression is observed in terms of S_{21} .

To demonstrate the performance improvement of the presented design over other state-of-the-art ones, a comparison table is given in Table II. In addition, using the method presented in [5], the unloaded quality factor (Q_u) of the filter is also given as a benchmark to evaluate the overall potential of the filter. As can be seen, comparing with the works presented in [13], [26] and [27], this work uses the same technology node for implementation and operates in a similar frequency band, but achieves better insertion loss with significantly reduced die area.

IV. CONCLUSIONS

In this work, a novel approach that can be used for miniaturized passive-device design, in particular a resonator and BPF, is presented. To qualitatively demonstrate the principle of the presented approach, simplified LC-equivalent circuit models for both the resonator and filter are given to investigate their transmission characteristics. The impact of using different combinations of inductance and capacitance is also investigated. Based on the investigation, the dimensions of both passive devices are optimized in a quantitative way using an EM simulator. To further prove that the presented approach is feasible in practice, both devices are fabricated in a standard 0.13- μ m (Bi)-CMOS technology. A reasonable agreement between the EM simulated and measured results is obtained. The sizes of both devices without pads are only 0.012 mm². In addition, the insertion loss of the designed filter is 1.7 dB, while the harmonic suppression is more than 20 dB at 66.75 GHz. According to the overall performances of the

designed devices, it can be concluded that this approach is particularly suitable for miniaturized MMIC design in silicon-based technologies.

REFERENCES

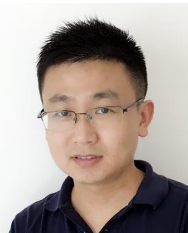
- [1] T. Dinc, A. Chakrabarti and H. Krishnaswamy, "A 60 GHz CMOS full-duplex transceiver and link with polarization-based antenna and RF cancellation," *IEEE J. Solid-State Circuits*, vol. 51, no. 5, pp. 1125–1140, May 2016.
- [2] A. Natarajan, S. K. Reynolds, M.-D. Tsai, S. T. Nicolson, J.-H. C. Zhan, D. G. Kam, D. Liu, Y. -L. O. Huang, A. Valdes-Garcia, and B. A. Floyd, "A fully-integrated 16-element phased-array receiver in SiGe BiCMOS for 60 GHz communications," *IEEE J. Solid-State Circuits*, vol. 46, no. 5, pp. 1059–1075, May 2011.
- [3] A. Tomkins, P. Garcia, and S. P. Voinigescu, "A passive W-band imaging receiver in 65 nm bulk CMOS," *IEEE J. Solid-State Circuits*, vol. 45, no. 10, pp. 1981–1991, Oct. 2010.
- [4] T. Cheung and J. R. Long, "Shielded passive devices for silicon-based monolithic microwave and millimeter-wave integrated circuits," *IEEE J. Solid-State Circuits*, vol. 41, no. 5, pp. 1183–1200, May 2006.
- [5] A. -L. Franc, E. Pistono, D. Gloria and P. Ferrari, "High-performance shielded coplanar waveguides for the design of CMOS 60-GHz bandpass filters," *IEEE Trans. Electron Device*, vol. 59, no. 5, pp. 1219–1226, May 2012.
- [6] J. R. Long, Y. Zhao, W. Wu, M. Spirito, L. Vera and E. Gordon, "Passive circuit technologies for mm-wave wireless systems on silicon," *IEEE Trans. Circuits Syst. I, Reg. Papers*, vol. 59, no. 8, pp. 1680–1693, Aug. 2012.
- [7] K. Ma, S. Mou, K. S. Yeo and W. M. Lim, "A cross-coupled LPF topology and design for millimeter-wave RFIC applications," *IEEE Trans. on Electron Devices*, vol. 59, no. 11, pp. 2902–2909, Nov. 2012.
- [8] Y. Wu, X. Ding, M. Ismail and H. Olsson, "RF bandpass filter design based on CMOS active inductors," *IEEE Trans. Circuits Syst. II*, vol. 50, no. 12, pp. 942–949, Dec. 2003.
- [9] L. Nan, K. Mouthaan, Y. Z. Xiong, J. Shi, S. C. Rustagi and B. L. Ooi, "Design of 60- and 77-GHz narrow-bandpass filters in CMOS technology," *IEEE Trans. Circuits Syst. II Exp. Briefs*, vol. 55, no. 8, pp. 738–742, Aug. 2008.
- [10] S. Sun, J. Shi, L. Zhu, S. C. Rustagi, and K. Mouthaan, "Millimeterwave bandpass filters by standard 0.18- μ m CMOS technology," *IEEE Electron Device Lett.*, vol. 28, no. 3, pp. 220–222, Mar. 2007.
- [11] D. M. Pozar, *Microwave Engineering*. New York, NY, USA: Wiley, 2009.
- [12] K. Ma, S. Mou and K. S. Yeo, "Miniaturized 60-GHz on-chip multimode quasi-elliptical bandpass filter," *IEEE Electron. Devices Lett.*, vol. 34, no. 8, pp. 945–947, Aug. 2013.
- [13] S. Chakraborty, *et al.*, "A broadside-coupled meander-line resonator in 0.13- μ m SiGe technology for millimetre-wave application," *IEEE Electron Devices Lett.*, vol. 37, no. 3, pp. 329–331, Mar. 2016.
- [14] C. -C. Tang, C. -H. Wu and S. -I. Liu, "Miniature 3-D inductors in standard CMOS process," *IEEE J. Solid-State Circuits*, vol. 37, no. 4, pp. 471–480, Apr. 2002.
- [15] W. Z. Chen, W. H. Chen and K. C. Hsu, "Three-dimensional fully symmetric inductors, transformer, and balun in CMOS technology," *IEEE Trans. Circuits Syst. I, Reg. Papers*, vol. 54, no. 7, pp. 1413–1423, Jul. 2007.

- [16] M. K. Chirala, X. Guan and C. Nguyen, "Integrated multilayered on-chip inductors for compact CMOS RFICs and their use in a miniature distributed low-noise-amplifier design for ultra-wideband applications," *IEEE Trans. Microw. Theory Tech.*, vol. 56, no. 8, pp. 1783-1789, Aug. 2008.
- [17] S. -C. Chang, Y. -M. Chen, S. -F. Chang, Y. -H. Jeng, C. -L. Wei, C. -H. Huang and C. -P. Jeng, "Compact millimeter-wave CMOS bandpass filters using grounded pedestal stepped-impedance technique," *IEEE Trans. Microw. Theory Tech.*, vol. 58, no. 12, pp. 3850-3859, Dec. 2010.
- [18] L. -K. Yeh, C. -Y. Chen and H. -R. Chuang, "A millimeter-wave CPW CMOS on-chip bandpass filter using conductor-backed resonators," *IEEE Electron Devices Lett.*, vol. 31, no. 5, pp. 399-401, May 2010.
- [19] Y. Shang, H. Yu, D. Cai, J. Ren and K. S. Yeo, "Design of high-Q millimeter-wave oscillator by differential transmission line loaded with metamaterial resonator in 65-nm CMOS," *IEEE Trans. Microw. Theory Tech.*, vol. 61, pp. 1892-1902, May 2013.
- [20] I. C. H. Lai, Y. Kambayashi and M. Fujishima, "60-GHz CMOS down-conversion mixer with slow-wave matching transmission lines," *Proc. IEEE Asian Solid-State Circuits Conf.*, pp. 195-198, Nov. 2006.
- [21] J. J. Lee and C. S. Park, "A slow-wave microstrip line with a high-Q and a high dielectric constant for millimeter-wave CMOS application," *IEEE Microw. Wireless Componen. Lett.*, vol. 20, no. 7, pp. 381-383, Jul. 2010.
- [22] K. Kim and C. Nguyen, "An ultra-wideband low-loss millimeter-wave slow-wave Wilkinson power divider on 0.18- μm SiGe Bi-CMOS process," *IEEE Microw. Wireless Componen. Lett.*, vol. 25, no. 5, pp. 331-333, May 2015.
- [23] A.-L. Franc, E. Pistono, N. Corrao, D. Gloria, P. Ferrari, "Compact high-Q low-loss mmW transmission lines and power splitters in RF CMOS technology," *Proc. Microw. Symp. Dig.*, pp. 1-4, June 2011.
- [24] A.-L. Franc, E. Pistono, G. Meunier, D. Gloria, P. Ferrari, "A lossy circuit model based on physical interpretation for integrated shielded slow-wave CMOS coplanar waveguide structures," *IEEE Trans. Microw. Theory Techn.*, vol. 61, no. 2, pp. 754-763, Feb. 2013.
- [25] A. Bautista, A. -L. Franc, P. Ferrari, "Accurate parametric electrical model for slow-wave CPW and application to circuits design," *IEEE Trans. Microw. Theory Techn.*, vol. 6, no. 4, pp. 625-636, June. 2016.
- [26] Y. Zhong, Y. Yang, X. Zhu, E. Dutkiewicz, K. M. Shum, and Q. Xue, "An on-chip bandpass filter using a broadside-coupled meander line resonator with a defected-ground structure," *IEEE Electron Device Lett.*, vol. 38, no. 5, pp. 626-629, May 2017.
- [27] Y. Yang, H. Liu, Z. J. Hou, X. Zhu, E. Dutkiewicz, and Q. Xue, "Compact on-chip bandpass filter with improved in-band flatness and stopband attenuation in 0.13- μm (Bi)-CMOS technology," *IEEE Electron Device Lett.*, vol. 38, no. 10, pp. 1359-1362, Oct. 2017.
- [28] L. -K. Yeung, K. -L. Wu and Y. -E. Wang, "Low-temperature cofired ceramic filters for RF applications," *IEEE Microw. Mag.*, vol. 9, no. 5, pp. 118-128, Oct. 2008.



He Zhu received the B.Sc degree and M.Eng degree from South China University of Technology, Guangzhou, China, and Ph.D. degree in Electrical Engineering from the School of ITEE, University of Queensland, Brisbane, Australia. He is currently a Post-doctoral Research Fellow with Global Big Data Technologies Centre (GBDTC), University of Technology Sydney (UTS), Australia. His research

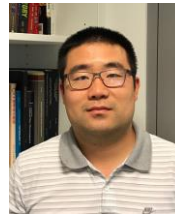
interests include development of radio frequency integrated circuits and systems, passive and tunable microwave and mm-wave devices, and beamforming networks for antenna arrays.



Yang Yang (S'11-M'14-SM'17) was born in Bayan Nur, Inner Mongolia, China and received the PhD degree from Monash University, Melbourne, Australia, in 2013. From July 2012 to April 2015, he was an Asia Pacific GSP Engineer at Rain Bird and a Global GSP Success Award holder of the year 2014. From April 2015 to April 2016, he served as a Senior Research Associate with Department of Engineering, Macquarie University, Sydney, Australia. From April 2016 to December 2016, he was a Research Fellow

with State Key Laboratory of Millimeter-Waves, City University of Hong Kong. In the same year, he has been involved in National Basic Research Program of China (973 Program) and appointed as an honorary research

fellow with Shenzhen Institute, City University of Hong Kong. In December 2016, Dr. Yang joined University of Technology Sydney, Australia, as a lecturer. His research interests include RFIC, microwave and millimeter-wave circuits and systems, reconfigurable antennas, wearable antennas and wearable medical sensing devices and systems. He is a current Associate Editor of IEEE ACCESS.



Xi Zhu received the B.E. (Hons.) and PhD from University of Hertfordshire (UH), Hertfordshire, UK, in 2005 and 2008, respectively. He is currently a Lecturer with the School of Computing and Communication, University of Technology Sydney, NSW, Australia. His research activities mainly involve in the areas of analogue baseband, radio frequency (RF) and mm-wave circuits and systems designs. He has co-authored over 80 refereed publications in the above-mentioned fields.



Yichuang Sun (M'90-SM'99) received the B.Sc. and M.Sc. degrees from Dalian Maritime University, Dalian, China, in 1982 and 1985, respectively, and the Ph.D. degree from the University of York, York, U.K., in 1996, all in communications and electronics engineering. He is currently a Professor and HoD with the School of Engineering and Technology of the University of Hertfordshire, UK. His research interests are mainly in the areas of wireless and mobile communications and RF and analogue circuits. He has published over 300 papers and contributed 10 chapters in edited books. He has also published 4 text and research books: Continuous-time Active Filter Design (CRC Press, USA, 1999), Design of High frequency Integrated Analogue Filters (IEE Press, UK, 2002), Wireless Communication Circuits and Systems (IET Press, 2004), and Test and Diagnosis of Analogue, Mixed-signal and RF Integrated Circuits - the Systems on Chip Approach (IET Press, 2008).

He was a Series Editor of IEE Circuits, Devices and Systems Book Series (2003-2008). He has been Associate Editor of IEEE Transactions on Circuits and Systems I: Regular Papers (2010-2011, 2016-2017, 2018-2019). He is also Editor of ETRI Journal, Journal of Semiconductors and some others. He was Guest Editor of 8 IEEE and IEE/IET journal special issues: High-frequency Integrated Analogue Filters in IEE Proc. Circuits, Devices and Systems (2000), RF Circuits and Systems for Wireless Communications in IEE Proc. Circuits, Devices and Systems (2002), Analogue and Mixed-Signal Test for Systems on Chip in IEE Proc. Circuits, Devices and Systems (2004), MIMO Wireless and Mobile Communications in IEE Proc. Communications (2006), Advanced Signal Processing for Wireless and Mobile Communications in IET Signal Processing (2009), Cooperative Wireless and Mobile Communications in IET Communications (2013), Software-Defined Radio Transceivers and Circuits for 5G Wireless Communications in IEEE Transactions on Circuits and Systems-II (2016), and IEEE International Symposium on Circuits and Systems in IEEE Transactions on Circuits and Systems-I (2016). He has also been widely involved in various IEEE technical committee and international conference activities.



Sai-Wai Wong (S'06-M'09-SM'14) received the B.S degree in electronic engineering from the Hong Kong University of Science and Technology, Hong Kong, in 2003, and the M.Sc and Ph.D. degrees in communication engineering from Nanyang Technological University, Singapore, in 2006 and 2009, respectively.

From July 2003 to July 2005, he was the Lead the Engineering Department in mainland of China with two manufacturing companies in Hong Kong. From 2009 to 2010, he was a Research Fellow with the Institute for Infocomm Research, Singapore. Since 2010, he was an Associate Professor and became a Full Professor with the School of Electronic and Information Engineering, South China University of Technology, Guangzhou, China. In 2016, he was a Visiting Professor with the City University of Hong Kong, Hong Kong. Since 2017, he is a Full Professor in College of Information, Shenzhen University, Shenzhen, China. His current research interests include RF/microwave circuit and antenna design. Dr. Wong was a recipient of the New Century Excellent Talents in University (NCET) Award in 2013 and the Shenzhen Overseas High-Caliber Personnel Level C in 2018. He is a Reviewer for several top-tier journals.